Available online at www.sciencedirect.com
ScienceDirect
Combustion and Flame 154 (2008) 546–556
Combustion and Flame
www.elsevier.com/locate/combustflame

# Soot inception limits in laminar diffusion flames with application to oxy–fuel combustion

B.M. Kumfer [1], S.A. Skeen, R.L. Axelbaum *

*Department of Energy, Environment, and Chemical Engineering, Washington University in St. Louis, St. Louis, MO 63130, USA*

Received 3 October 2007; received in revised form 6 February 2008; accepted 10 March 2008

Available online 28 May 2008

**Abstract**

For diffusion flames, the combination of oxygen enrichment and fuel dilution results in an increase in the stoichiometric mixture fraction, $Z_{st}$, and alters the flame structure, i.e., the relationship between the local temperature and the local gas composition. Increasing $Z_{st}$ has been shown to result in the reduction or even elimination of soot. In the present work, the effects of variable $Z_{st}$ on soot inception are investigated in *normal* and *inverse* coflow flames, using ethylene as the fuel. Use of the inverse coflow flame underscores the validity of these concepts, since the convective field in the inverse flame directs particles into the fuel-rich region. Sooting limits based on particle luminosity are measured as a function of $Z_{st}$. The sooting limit is obtained by varying the amount of inert gas until soot appears above a predefined height. For each limit flame, the adiabatic flame temperature is calculated and the flame temperature at the half-height is measured. The flame temperature at the sooting limit is found to increase with $Z_{st}$ for both normal and inverse flames. The effects of residence time are also investigated, and the sooting limit inception temperature is found to be dependent on fuel stream velocity for both the normal and inverse configurations. A simple model applicable to oxy–fuel combustion is presented which describes how increasing $Z_{st}$ results in the reduction and ultimately elimination of soot. This model assumes that soot inception can only occur in a region where critical values for species, temperature, and residence time are met. The soot inception region is shown to be bounded by two isotherms: a low-temperature boundary that is a function of residence time, and a high-temperature boundary that corresponds to the location of a critical local carbon-to-oxygen ratio. The effect of increasing $Z_{st}$ is to move the boundaries of the soot inception zone towards each other, until the zone is infinitely thin and thus the sooting limit is reached. By comparing the model to experimental data, a critical local C/O ratio of 0.53 and a sooting limit inception temperature of 1640 K (for a characteristic residence time of 22 ms) were determined for ethylene.


*Keywords:* Inverse flame; Coflow flame; Sooting limits; Oxy–fuel; Oxygen-enriched

## 1. Introduction

For a typical fuel/air diffusion flame, it is generally accepted that soot inception occurs as a consequence of fuel pyrolysis, which leads to the formation of PAH and soot particles. Given that the chemistry of soot in-

* Corresponding author. Fax: +1 314 935 4014.
*E-mail address:* rla@wustl.edu (R.L. Axelbaum).
[1] Current address: Department of Mechanical and Aeronautical Engineering, University of California, Davis, CA 95616, USA.

0010-2180/$ – see front matter 
doi:10.1016/j.combustflame.2008.03.008

ception is high-activation-energy, soot inception will only occur if the local temperature and residence time are sufficiently high. The soot inception temperature, i.e., the temperature at which soot is first observed on the fuel side of the flame, has been measured in sooting diffusion flames [1–3]. Gomez et al. [1] measured the inception temperature along the centerline of the coflow flame for four different fuels and determined it to be approx. 1350 K, regardless of fuel type or level of dilution. Dobbins [4] proposed that the inception temperature can be predicted from an Arrhenius reaction equation, which describes the conversion of soot precursors to soot particles. Glassman [5] postulated that the distance between the incipient particle formation isotherm and the stoichiometric flame temperature isotherm controls the soot volume fraction. He further stated that this distance corresponds to the particle growth time before soot particle oxidation occurs at the flame, and thus the thermal diffusivity of the fuel or fuel additives has a direct effect on the soot growth time. Counterflow flame studies have also shown the importance of residence time on soot formation. For example, it has been observed that a sooting counterflow flame will become soot-free when the strain rate is increased. The limiting strain rate that results in a soot-free flame has been measured by Kennedy [6], Du et al. [7] and Lin and Faeth [8].

The local gas composition is also an important criterion for soot formation in diffusion flames. In the work of Du et al. [9], it was demonstrated that fuel dilution reduces soot. This effect was separated from the effects of temperature by using different inert gases, while maintaining constant flame temperature. Furthermore, it has been demonstrated that fuel dilution and oxygen enrichment can lead to a net reduction in soot formation, even at high temperatures. For example, a sooting fuel/air flame can be made blue (soot-free) by replacing air with oxygen and diluting the fuel while maintaining constant flame temperature [10]. The relative amounts of oxygen enrichment and fuel dilution can be quantified by the stoichiometric mixture fraction, $Z_{st}$, defined as $Z_{st} = (1 + Y_{F,0} W_O \upsilon_O / Y_{O,0} W_F \upsilon_F)^{-1}$, where $Y_{F,0}$ and $Y_{O,0}$ represent the fuel and oxidizer mass fractions at the inlet, $W_F$ and $W_O$ are the species molecular weights, and $\upsilon_F$ and $\upsilon_O$ are the fuel and oxygen stoichiometric coefficients, respectively. The influence of $Z_{st}$ on soot inception has been the subject of many investigations [8,10–13]. Lin and Faeth [8] suggested that changes in $Z_{st}$ affect soot formation through the variation in the velocity and direction of flow normal to the flame sheet, while Du and Axelbaum [10] and Sunderland et al. [11] have concluded that soot inception is affected by $Z_{st}$ primarily because of its influence on the relationship between the local temperature and the local gas composition in the soot zone.

In this work emphasis is placed on soot *inception*, which we consider to be the growth of gas-phase species culminating in the creation of a luminous soot particle. We will not consider phenomena occurring after particle inception, such as particle transport and surface oxidation. In previous studies, soot inception limits were measured as a function of $Z_{st}$ in counterflow flames [7], spherical microgravity flames [11], and normal coflow flames [14]. In each of these studies, the flame temperature at the sooting limit was found to increase linearly with $Z_{st}$ and this behavior was attributed to the variation in flame structure with $Z_{st}$. In other words, gas composition and its relationship to temperature play a primary role in governing soot inception. In addition, a theory for predicting the sooting limit data was evaluated, which assumes that soot inception can only occur when the local C/O ratio is equal to or above a critical value [11]. Values for the nonpremixed critical *local* C/O ratio were recently derived utilizing the normal coflow flame and, perhaps surprisingly, the sooting limit results agreed well with published results for the *global* C/O ratio for premixed flames for a variety of gaseous fuels [14]. However, these results were obtained with the assumption that the variation in residence time between flames had a secondary effect on the sooting limits.

The objective of this work is to expand the sooting limit model to include the effects of finite-rate soot chemistry and the characteristic residence time. In order to better examine these effects, both normal and inverse coflow flames are utilized. Normal flames are created by injecting fuel into a surrounding oxidizer stream, while inverse flames are created by injecting oxidizer into a surrounding fuel stream. While soot formation in the normal coflow flame has been well characterized, soot formation in the inverse flame has received less attention [15–20]. In the inverse flame, soot particles form in the fuel-rich region on the outside of the stoichiometric flame surface and they are not directed into the oxidizer stream by convection. Thus, the inverse flame is valuable for studying early-stage soot formation, since formation processes are well separated from oxidation processes [16]. More importantly for this work, the inverse flame has the added advantage that the flame height can be varied without varying the fuel flow rate, enabling one to separate effects from these parameters. Studies characterizing soot formation in the inverse flame were performed by Sidebotham and Glassman [15,16], who utilized gas chromatography, and Makel and Kennedy [17], who utilized light scattering. Vander Wal [18], Blevins et al. [19], and Oh et al. [20] performed studies on the early stages of soot inception in the inverse flame, while Kaplan and

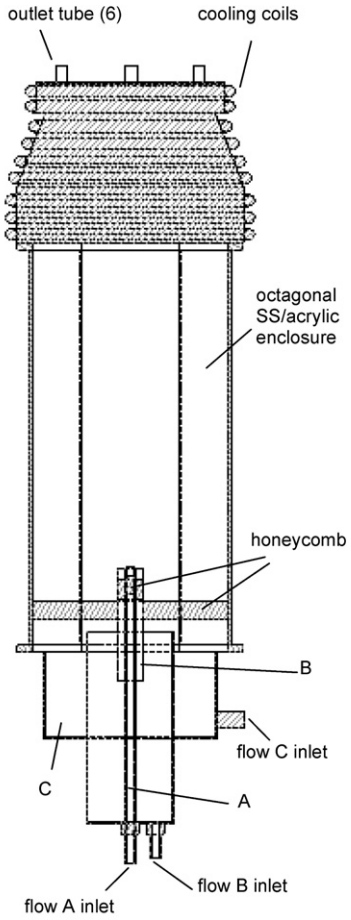


| Tube A, ID | Tube B, ID | Tube C,ID |
|---|---|---|
| 6.2 mm | 17 mm | 120 mm |

Fig. 1. Schematic diagram of burner for normal and inverse coflow flames.

Kailasanath [21] employed numerical simulations to compare flow-field effects on soot formation in normal and inverse flames.

## 2. Experimental

The experimental setup consists of a triaxial coflow burner surrounded by an octagonal stainless steel chimney with three of the steel panels replaced by acrylic windows for optical diagnostics as shown in Fig. 1. The inner, secondary, and tertiary tube diameters are 6.2, 17, and 120 mm, respectively. The third coannular flow is added to ensure that sufficient fuel is available within the chimney when it is operated in the inverse mode and to provide for an overventilated condition independent of the secondary stream velocity. The gas compositions exiting the outer tube (tube C) and the intermediate tube (tube B) are kept identical at all times. The outer flow rate is kept small, while the exit velocity of the intermediate stream can be increased as needed. In this way, when operating in the inverse mode, the velocity of the fuel stream adjacent to the oxidizer stream can be varied without introducing significantly more fuel into the system, which would result in safety concerns associated with exhausting large amounts of unburned fuel. Honeycomb is used in all streams to produce uniform and stable flows. The fuel ($C_2H_4$) and oxidizer mass fractions are controlled by dilution with nitrogen. Flow rates are measured with calibrated sonic nozzles. At the top of the chimney, the exhaust is forced through six outlet tubes and when operating in the inverse mode, any unburned fuel is immediately burned in room air with the aid of pilot flames.

The sooting limit is defined as the flame condition that leads to the disappearance of visible soot luminosity at a given location as observed using a cathetometer in a dark room. In a previous study by this group, the sooting limit as determined by soot luminosity was compared with the limit determined by the threshold of Rayleigh scattering of laser light from particles [7]. The sooting limits based on these two methods were found to be in good agreement, and in fact the visible soot luminosity method was found to be slightly more sensitive than the light scattering method. Thus, soot luminosity will be used to obtain the sooting limit. We observe the sooting limit at a fixed height of 8 mm, measured from the burner exit. The limit is obtained by varying the total amount of inert (nitrogen) at constant $Z_{st}$ until yellow luminosity is first perceptible at the 8 mm height. That is, above this height there is yellow luminosity in the flame, but below this height there is no yellow luminosity at any radial position in the flame. The adiabatic flame temperature for each sooting-limit flame is computed using the CEA chemical equilibrium code [22]. Photographs of both a normal and an inverse flame near the sooting limit are shown in Fig. 2. While not evident in the photograph, the soot appears orange to the naked eye in the inverse flame while it appears yellow in the normal flame. This difference in emission may be attributed to differences in particle temperature.

The flame temperature is measured in selected limit flames using a Pt–6%Rh/Pt–30%Rh thermocouple constructed from 50-μm wire. Corrections for radiative heat loss are made using the Nusselt number correlation for convective heat transfer to a spherical bead, with a measured diameter of 290 μm and assuming a bead emissivity equal to 0.22. Thermocouple temperatures in excess of approx. 2100 K are not obtainable due to the limits of the Pt–6%Rh/Pt–30% wire.


Fig. 2. Photographs of (a) normal and (b) inverse sooting limit flames. The sooting limit is observed at a height of 8 mm from the burner lip.

Measurements of the velocity field are taken using laser Doppler velocimetry (LDV). The flows are seeded with alumina particles manufactured by Alfa Aesar, which have a nominal size of 0.3 μm.

## 3. Results and discussion

For the first set of experiments, the flame height is held constant and the flow rate from the central tube is varied. In the second set, the fuel flow rate is held constant, resulting in a variable flame height (for the normal flame). The input parameters for all of the limit flames are summarized in Table 1, where $V_{e,F}$ and $V_{e,O}$ are the mean fuel and oxidizer exit velocities, which are determined by dividing the volumetric flow rate by the exit area, and $Y_{F,0}$ and $Y_{O,0}$ are the fuel and oxygen mass fractions at the burner outlet, respectively.

### 3.1. Constant flame height

For this set of experiments, the flame height is maintained at $16 \mp 1$ mm. When $Z_{st}$ is varied in the normal flame configuration, a constant 16-mm flame height can only be obtained if the fuel stream flow rate is varied, since flame height is a function of both $Z_{st}$ and fuel flow rate. For inverse flames, flame height is controlled by the oxidizer stream flow rate, and thus the fuel stream flow rate can be held constant for all stoichiometric mixture fractions. The flow rate of the oxidizer stream in the inverse flame is found to have no effect on soot inception in the region of interest for the flow rates considered in this study. Since the fuel flow rate can be held constant and the oxidizer flow rate does not affect the sooting limit, only buoyancy should have an impact on residence time for the sooting limit data for the inverse flames.

Since the sooting limit is defined for a height of 8 mm, these flames may be described as *half blue* [14]. In Fig. 3, the adiabatic flame temperature corresponding to the half-blue condition is plotted as a function of $Z_{st}$. In addition, the measured flame temperature at the flame half-height (8 mm) is plotted. The normal and inverse data are shown together for comparison. For both normal and inverse flames, the sooting limit flame temperature increases with $Z_{st}$ by as much as 500 °C. This is the case for both flame types despite the fact that the direction of convection for the normal flame is opposite that of the inverse flame. The suppression of soot with increasing $Z_{st}$ is consistent with results in counterflow flames [8,12], spherical microgravity flames [11] and normal coflow flames [14]. The results further demonstrate the usefulness of oxygen-enriched combustion in combination with fuel dilution as a tool for optimizing temperature while minimizing soot formation.

As demonstrated in Fig. 3, the limits for the normal and inverse flames are similar for $0.2 < Z_{st} < 0.4$. Beyond $Z_{st} = 0.4$, the limits for the normal flames deviate from those of the inverse flame. As shown in Table 1, at $Z_{st} = 0.20$ the mean fuel stream exit velocities for the normal and inverse flames are nearly identical, while for larger $Z_{st}$ the differences increase by up to 300%.

The increased fuel stream velocity in the normal flame may reduce the characteristic residence time for soot formation in coflow flames. Decreasing residence time results in a reduction of soot, as demonstrated by the aforementioned counterflow studies [7,8]. Thus, the deviation of the normal flame limit data from the inverse flame data may be a result of reduced residence time. The flow field and thus the residence time may be affected by both exit velocity and acceleration due to buoyancy. The influence of buoyancy can be assessed from the Richardson number, Ri, defined as

$$\mathrm{Ri} = gL(T_f - T_0)/\left(T_0 V^2\right), \tag{1}$$

where $g$ is the acceleration of gravity, and $T_f$ and $T_0$ are the flame temperature and free stream temperature, respectively. Since we are concerned with the effects of buoyancy on the soot inception limit, we choose $L = 8$ mm (soot inception height) and $V = V_{e,F}$. The Richardson numbers for the extreme cases (low and high $Z_{st}$) are given in Table 2. Indeed, for most of the flames in this study, $\mathrm{Ri} \gg 1$, indicating that the flow field is dominated by buoyancy. Thus, the exit velocity alone is insufficient to characterize

Table 1
Input parameters of sooting limit flames

| Normal coflow | | | | | Inverse coflow | | | | |
|---|---|---|---|---|---|---|---|---|---|
| $Z_{st}$ | $Y_{F,0}$ | $Y_{O,0}$ | $V_{e,F}$ [cm/s] | $V_{e,O}$ [cm/s] | $Z_{st}$ | $Y_{F,0}$ | $Y_{O,0}$ | $V_{e,F}$ [cm/s] | $V_{e,O}$ [cm/s] |
| Exp. #1: Constant flame height | | | | | | | | | |
| 0.20 | 0.259 | 0.222 | 11 | 17 | 0.20 | 0.259 | 0.222 | 11 | 45 |
| 0.25 | 0.215 | 0.245 | 14 | 17 | 0.25 | 0.215 | 0.245 | 11 | 42 |
| 0.30 | 0.185 | 0.272 | 18 | 17 | 0.30 | 0.185 | 0.272 | 11 | 38 |
| 0.35 | 0.163 | 0.301 | 21 | 17 | 0.35 | 0.163 | 0.301 | 11 | 34 |
| 0.40 | 0.148 | 0.338 | 24 | 17 | 0.40 | 0.148 | 0.338 | 11 | 31 |
| 0.45 | 0.138 | 0.387 | 28 | 17 | 0.45 | 0.136 | 0.379 | 11 | 29 |
| 0.50 | 0.133 | 0.454 | 31 | 17 | 0.50 | 0.125 | 0.429 | 11 | 24 |
| 0.55 | 0.129 | 0.541 | 37 | 17 | 0.55 | 0.118 | 0.495 | 11 | 18 |
| 0.60 | 0.126 | 0.648 | 47 | 17 | 0.60 | 0.111 | 0.568 | 11 | 17 |
| 0.65 | 0.126 | 0.799 | 48 | 17 | 0.65 | 0.105 | 0.668 | 11 | 14 |
| Exp. #2: Constant mean exit velocity | | | | | | | | | |
| 0.17 | 0.314 | 0.218 | 43 | 43 | 0.24 | 0.220 | 0.244 | | 30 |
| 0.21 | 0.255 | 0.238 | 43 | 43 | 0.32 | 0.179 | 0.288 | | 30 |
| 0.24 | 0.232 | 0.249 | 43 | 43 | 0.39 | 0.150 | 0.330 | | 30 |
| 0.30 | 0.195 | 0.288 | 43 | 43 | 0.42 | 0.150 | 0.364 | | 30 |
| 0.36 | 0.168 | 0.324 | 43 | 43 | 0.45 | 0.145 | 0.404 | | 30 |
| 0.42 | 0.154 | 0.377 | 43 | 43 | 0.47 | 0.140 | 0.422 | | 30 |
| 0.46 | 0.145 | 0.428 | 43 | 43 | 0.51 | 0.134 | 0.480 | | 30 |
| 0.55 | 0.139 | 0.587 | 43 | 43 | 0.56 | 0.128 | 0.553 | | 30 |
| 0.59 | 0.133 | 0.647 | 43 | 43 | 0.61 | 0.125 | 0.680 | | 30 |
| | | | | | 0.66 | 0.122 | 0.800 | | 30 |
| | | | | | 0.73 | 0.110 | 1.000 | | 30 |

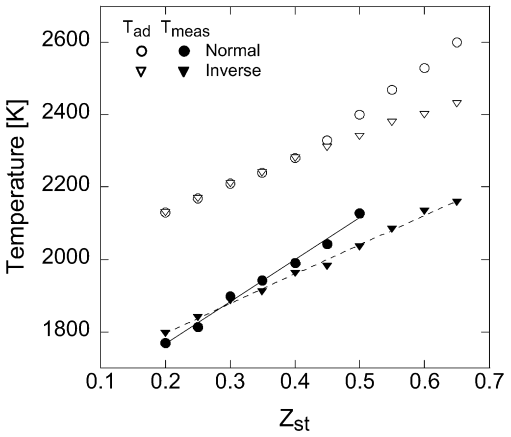


Fig. 3. Sooting limit flame temperature vs stoichiometric mixture fraction for normal and inverse flames. Case 1: Constant flame height of 16 mm.

the residence time for soot inception in these flames. The high-$Z_{st}$ normal flame, in which the Ri is on the order of unity, is an exception to this. In this case, the exit velocity is sufficiently high so that buoyancy effects are reduced and the residence time begins to scale with $L/V$.

To obtain a more accurate characterization of residence time, the vertical component of velocity in the region of soot inception was measured by LDV. These results are also summarized in Table 2. Using these data, the residence time, $\tau$, for soot inception is found by tracking a parcel of fuel from the burner exit to the location of soot inception, and is calculated from

$$\tau = \int_0^{8\text{ mm}} 1/V(z)\,\mathrm{d}z. \tag{2}$$

It is assumed that the vertical component of velocity increases linearly with height, $z$. Earlier measurements of the entire flow field taken in similar half-blue coflow flames [23] indicated that this is a good approximation. As can be seen from Table 2, the residence time in the normal flame decreases dramatically as $Z_{st}$ is increased, while $\tau$ is nearly constant (within 6%) for the inverse flame over the entire span of $Z_{st}$. This is strong evidence that the differences between the normal and inverse sooting limits observed in Fig. 3 can be attributed to residence time.

Table 2
Selected properties of sooting limit flames

| | $Z_{st}$ | $V_e$ [cm/s] | $V_{8\text{ mm}}$ [cm/s] | Ri | $\tau$ [ms] |
|---|---|---|---|---|---|
| Normal | 0.20 | 11 | 66 | 32 | 26.1 |
| | 0.65 | 48 | 100 | 2 | 11.3 |
| Inverse | 0.20 | 11 | 87 | 32 | 21.8 |
| | 0.65 | 11 | 80 | 40 | 23.0 |

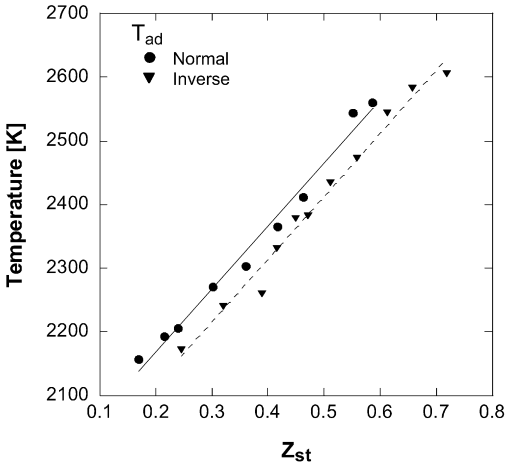


Fig. 4. Sooting limit flame temperature vs stoichiometric mixture fraction for normal and inverse flames. Case 2: Constant gas exit velocity.

### 3.2. Constant exit velocity

Measurements of sooting limits were performed in a second set of experiments in which the mean exit velocities of the fuel and oxidizer streams were set equal and held constant as $Z_{st}$ is varied. While this causes the flame length to vary, the sooting limit is still identified at a height of 8 mm from the burner lip throughout the experiments. The flow rates are kept large so that $\mathrm{Ri} = O(1)$ and the effects of buoyancy at a height of 8 mm are minimized. In this way, the residence time is held constant as $Z_{st}$ is varied and velocity gradients normal to the flame surface are minimized. For the normal flames, the mean exit velocity is 43 cm/s. For the inverse flames, a mean exit velocity of 43 cm/s could not be attained without flame fluctuations; thus for these flames a mean exit velocity of 30 cm/s is used. Since some of the flames in these experiments are quite tall, a 12.7-mm stainless steel tube is placed above the flame at a height of approx. 50 mm from the burner to quench and stabilize the top portion of the flame and minimize flame fluctuations. The flames were observed with and without the quenching tube to ensure that the tube caused no visible effect on the sooting limit. The sooting limit results for constant residence time are shown in Fig. 4.

In this case, the slope of the best-fit line through the data for the normal flame is nearly equal to that of the inverse flame. This implies that the effects of $Z_{st}$ on soot inception are the same, regardless of the geometric differences, provided that the residence time is fixed. The intercept of the best-fit line is larger for the normal flame, and this is attributed to the overall shorter residence time associated with these flames.

In the following section, we present a simple model for sooting limits that combines the residence time effects demonstrated above with the idea of a critical local C/O ratio, as proposed by Sunderland et al. [11].

### 3.3. Modeling the sooting limit

The region conducive to soot inception in a nonpremixed flame can be considered bounded by two locations in the fuel side. One is at a low temperature, below which the chemistry of soot inception is too slow; the other is at a higher temperature, where the local gas composition is not favorable for soot inception due to the presence of oxygen-containing species. This concept of two boundaries has similarities to that proposed in the work of Glassman [5]. In that work it was assumed that the high-temperature sooting limit boundary was coincident with the location of stoichiometric flame temperature.

For simplicity, we assume that the onset of soot can be described by a set of reactions that are overall first-order in fuel, so that they can be represented by

$$\text{fuel} \xrightarrow{k} \text{soot}. \tag{3}$$

The reaction rate coefficient, $k$, is assumed to be of Arrhenius form, and the change in soot mass fraction, $Y_{\text{soot}}$, due to soot formation is written as

$$w = \frac{\mathrm{d}Y_{\text{soot}}}{\mathrm{d}t} = A \cdot \exp\left(-\frac{E}{R \cdot T}\right) \cdot Y_{\text{fuel}}, \tag{4}$$

where $E$ is the activation energy for soot inception, $R$ is the gas constant, and $Y_{\text{fuel}}$ is the local fuel mass fraction. The local fuel mass fraction can be related to the local temperature by imposing the classical Burke–Schumann assumptions and utilizing coupling functions. Through this approach, the local soot formation rate can be written as a function of temperature only. Thus for any flame defined by the flame temperature, $T_f$, and $Z_{st}$ we can write

$$w = A \cdot \exp\left(-\frac{E}{RT}\right) \cdot \frac{(T_f - T)}{Z_{st}} \cdot \frac{c_p}{q_c}, \tag{5}$$

where $c_p$ denotes the constant gas specific heat and $q_c$ the heat of combustion. Also note that for given freestream fuel and oxidizer concentrations, $Z_{st}$ and $T_f$ are uniquely defined.

We now identify $T_{\text{kin}}$ as the temperature above which the kinetics are favorable for soot formation. More specifically, at the location of $T_{\text{kin}}$ there is a barely detectable luminous quantity of soot, and this critical soot mass fraction is denoted as $Y_{\text{soot, c}}$. It is assumed that the time required to reach $Y_{\text{soot, c}}$ is proportional to the characteristic residence time, $\tau$, and by considering the mean soot formation rate over the soot inception region, $W = 1/L \int w \, \mathrm{d}x$, we can write

the following:

$$Y_{\text{soot, c}} \propto \tau \cdot W. \tag{6}$$

By substituting Eq. (6) into Eq. (5) and lumping the constants together into a new constant, $C_0$, we obtain

$$T_f = T_{\text{kin}} + \frac{Z_{\text{st}}}{C_0 \cdot \tau} \exp\left(\frac{E}{RT_{\text{kin}}}\right). \tag{7}$$

Thus for any flame defined by $Z_{\text{st}}$, $T_f$, and $\tau$, $T_{\text{kin}}$ can be predicted provided that $C_0$ can be obtained for one set of conditions.

The boundary on the high-temperature side of the soot formation zone corresponds to the location at which the local gas composition is no longer favorable for soot formation, since sufficient oxygen-containing species exist. It has been proposed that soot formation is no longer favorable when the local C/O ratio is less than some critical value, $(\text{C/O})_{\text{cr}}$ [9]. Sunderland et al. employed the Burke–Schumann approach and derived Eq. (8) below, which relates the local temperature to the local C/O ratio at the high-temperature boundary,

$$T_f = T_{\text{C/O}} + (T_{\text{C/O}} - T_0) \cdot Z_{\text{st}} \cdot \left[2 \cdot \frac{m + n/4}{m} \cdot (\text{C/O})_{\text{cr}} - 1\right], \tag{8}$$

where $T_{\text{C/O}}$ is the local temperature at this soot formation boundary and $(\text{C/O})_{\text{cr}}$ is the critical carbon-to-oxygen ratio. In Eq. (8), $m$ represents the number of carbon atoms and $n$ the number of hydrogen atoms in the fuel $C_mH_n$, and $T_0$ denotes the inlet temperature.

Based on Eqs. (7) and (8) above, the sooting limit occurs when the low-temperature boundary and the high-temperature boundary converge, i.e., $T_{\text{C/O}} = T_{\text{kin}}$. For a flame at its sooting limit, a decrease in $Z_{\text{st}}$ or an increase in either residence time or flame temperature will result in the appearance of luminous soot. We define $T_{\text{lim}}$ as the temperature at the location where soot is first observed in a limit flame such that at the sooting limit $T_{\text{lim}} = T_{\text{kin}} = T_{\text{C/O}}$.

For the model to be used, the pre-exponential constant ($C_0$) in Eq. (7) must first be determined. Once this is known, $T_{\text{kin}}$ can be predicted for a given residence time and $Z_{\text{st}}$. The amount of inert in the freestreams must also be provided as this will affect the flame temperature. The pre-exponential factor $C_0$ and $T_{\text{kin}}$ in Eq. (7) can be obtained empirically. Since $\tau$ and $T_f$ were measured in the inverse flames of constant flame height, this data can be substituted into Eq. (7). The overall activation energy for soot inception is available in the literature. Du et al. measured an activation energy for ethylene of 31 kcal/mol [24]. Equation (7) can then be solved for $C_0$ at each experimental data point by letting $T_{\text{kin}}$ vary until the standard deviation of $C_0$ is minimized. The best fit for the constant-flame-height, inverse-flame data was obtained for $C_0 = 780\ \text{K}^{-1}\,\text{s}^{-1}$ and $T_{\text{kin}} = 1640$ K. Since these are limit flames, we can write $T_{\text{kin}} = T_{\text{lim}}$ and thus we conclude that $T_{\text{lim}} = 1640$ K.

Using a thermocouple, Gomez et al. [1] measured the inception temperature along the centerline of a heavily sooting laminar coflow flame and obtained a temperature of approximately 1350 K for a variety of fuels. This is in contrast to the work of Glassman et al. [25], who studied heavily diluted ethylene/air coflow flames where soot luminosity was no longer visible at the tip. They measured the temperature where luminosity last appeared and found it to be approximately 1600 K. Note that the measurements of soot inception temperature in these two studies were obtained using different criterion. Gomez et al. measured the centerline temperature where soot was first observed in sooting flames, which is consistent with our definition of $T_{\text{kin}}$, whereas Glassman et al. measured the temperature where soot appears in a flame at its sooting limit, or $T_{\text{lim}}$. The latter is more relevant to this work and the value of ca. 1600 K corresponds well with our predicted value of 1640 K.

With $T_{\text{lim}}$ known, Eq. (8) can now be solved for the critical C/O ratio at each experimental data point. Letting $T_{\text{C/O}} = T_{\text{lim}} = 1640$ K, we obtain an average $(\text{C/O})_{\text{cr}}$ of 0.53 with a standard deviation of 0.005. The linear relationship between the flame temperature at the sooting limit and $Z_{\text{st}}$ predicted by the model is shown together with the experimental data from the inverse flame in Fig. 5, and the model is a good representation of the data. Interestingly, the value for $(\text{C/O})_{\text{cr}}$ is similar to, though slightly lower than, the global critical C/O ratio that is observed in ethylene premixed flames. Harris et al. [26] observed that for premixed flames, the critical C/O ratio varies from 0.55 to 0.64 in the temperature range of 1620–1840 K. The value of $(\text{C/O})_{\text{cr}}$ for ethylene obtained in this work is somewhat lower than the value obtained previously by this group in the study of normal coflow flames of constant flame height (0.53 compared to 0.60) [14]. This difference is likely due to the fact that the soot inception model of the previous work did not address the effects of variable residence time. The results in Fig. 3 demonstrate that the slope of the sooting limit line increases with $Z_{\text{st}}$ for the normal flames at constant flame height. As discussed, residence time decreases for these flames and thus the higher $Z_{\text{st}}$ flames are expected to have higher limit temperatures than they would if residence time were constant. The increase in slope will in turn result in an overprediction of $(\text{C/O})_{\text{cr}}$ if Eq. (8) is directly fitted to this sooting limit data, as it was in [14], and thus the value of $(\text{C/O})_{\text{cr}} = 0.6$ in [14] is believed to be an overprediction.

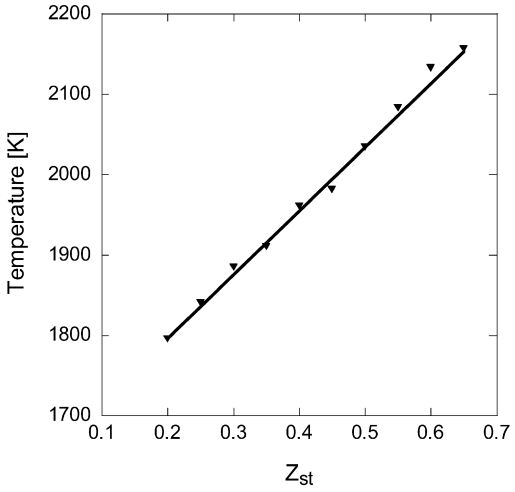


Fig. 5. Comparison of measured inverse flame sooting limits and the model (line) obtained with $E_a = 31$ kcal/mol; $C_0 = 780\ \mathrm{K}^{-1}\ \mathrm{s}^{-1}$, $\tau = 22.4$ ms and $(\mathrm{C/O})_{cr} = 0.53$.

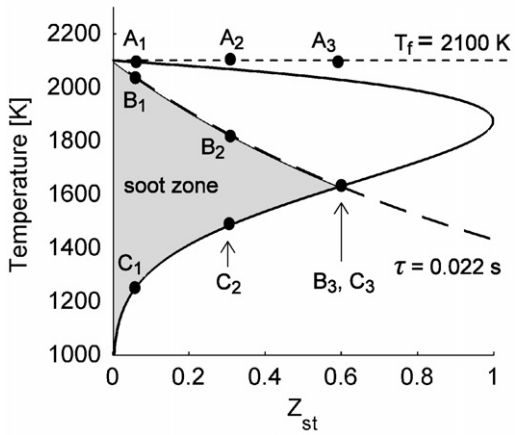


Fig. 6. Representation of the collapse of the soot formation zone with increasing $Z_{st}$.

Plotting Eqs. (7) and (8) in $Z_{st}$ space provides valuable insight into the effect of $Z_{st}$ on soot inception. Both $T_{kin}$ and $T_{C/O}$ are plotted in Fig. 6 as functions of $Z_{st}$ assuming a flame temperature of 2100 K and a residence time of 22 ms. The residence time was chosen to be similar to that of the inverse flame data in Table 2 but is for illustrative purposes only. To understand how to interpret Fig. 6, first consider the $T_{kin}$ curve (solid line). This curve represents simple Arrhenius kinetics that are first-order in fuel. The abscissa is the temperature on the fuel side of the flame, and if we consider a given $Z_{st}$, we see that soot will not form in the regions where temperature is low on the fuel side (e.g., below 1450 K at $Z_{st} = 0.3$). That is, below the solid line, even though there is a high concentration of fuel, the kinetics is too slow to form soot in the available residence time. As we cross the solid line, we move into a region where the temperature is sufficiently high to allow soot to form in the available time. The upper branch of the solid line represents a region very close to the peak temperature location where soot cannot form because the fuel concentration is too low, approaching zero at the flame. Of course, multistep kinetics would alter the details of this description, but this simple description yields the critical features associated with flame structure.

As we shall show below, the relevant branch on the $T_{kin}$ curve is the lower branch, as the upper branch is not realizable in practice. Consider the dashed curve that represents $T_{C/O}$, obtained from Eq. (8). Above $T_{C/O}$, soot cannot form because the C/O ratio is too low, i.e., there is too much oxygen available from oxygen-containing species relative to carbon from carbon-containing species. Also, as can be shown from Eq. (8), the temperature at which this critical C/O ratio occurs decreases with $Z_{st}$.

This reduction of $T_{C/O}$ with $Z_{st}$ is critical to understanding why high-$Z_{st}$ flames can be made to be intrinsically soot free for any strain rate, i.e., they can be "permanently" blue [8]. It can also be used to illustrate how, for a given residence time and flame temperature, a sooting limit can be achieved by increasing $Z_{st}$. To illustrate this, the results from the flame sheet model are plotted in mixture fraction space in Fig. 7. These figures correspond to the three flames considered in Fig. 6, which have identical flame temperatures and residence times but distinct stoichiometric mixture fractions. To begin this illustration, first consider Case 1 (as denoted by subscript 1) in Fig. 6, which represents a fuel/air flame with $Z_{st} = 0.064$ and a flame temperature of approximately 2100 K. Moving vertically from the $x$-axis to point $C_1$ in Fig. 6 is equivalent to moving along the temperature curve from right to left in mixture fraction space in Fig. 7a. At $C_1$ there are sufficient temperature, time, and fuel species for soot formation to occur on the fuel side of the flame, where the local temperature is approximately 1250 K. At any temperature lower than $C_1$ soot will not form because the chemistry is too slow. Moving vertically in Fig. 6 from $C_1$ to $B_1$, we pass through the broad soot zone associated with the fuel/air flame, until we reach the location in the flame where sufficient oxygen-containing species are available so that soot formation is no longer favored. At point $B_1$ the soot zone ends because the local C/O ratio is equivalent to the critical C/O ratio. We note also that the high-temperature soot zone boundary at $B_1$ is not coincident with the peak temperature location at $A_1$, although for low-$Z_{st}$ flames the two are relatively close. Thus, for low $Z_{st}$ flames our results compare well with Glassman's statement that soot particles begin forming at the nucleation bound-

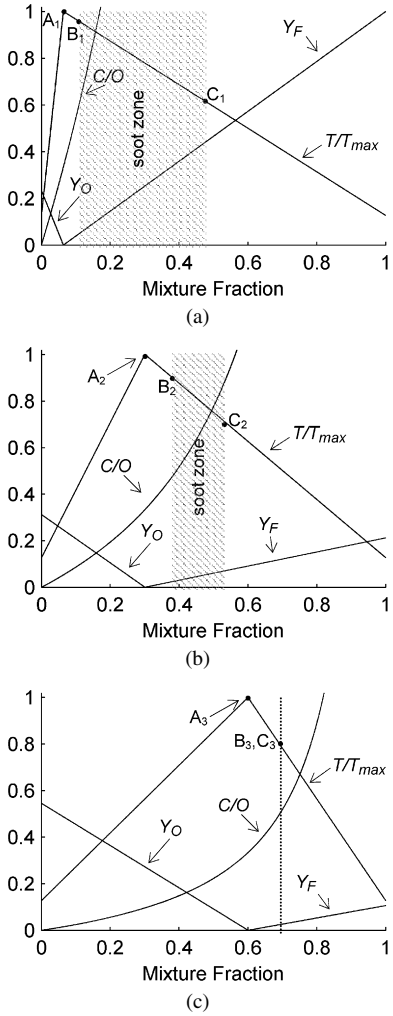


Fig. 7. Flame sheet model results for Cases 1, 2, and 3 from Fig. 6 showing shrinking of soot formation zone due to convergence of low-temperature ($T_{\text{kin}}$) and low C/O ratio (high-temperature $T_{\text{C/O}}$) boundaries.

ary and are consumed at the location of stoichiometric flame temperature [5]. As $Z_{\text{st}}$ increases, however, the high-temperature soot zone boundary moves away from the stoichiometric flame temperature location, as will be shown next. It is also noteworthy that the finite distance between the peak temperature and the high-temperature soot inception boundary predicted by the model indicates that a dead space should exist on the fuel side of the peak temperature, where no soot can form, as has been observed by Du [27].

Increasing $Z_{\text{st}}$ to 0.3 while maintaining the same flame temperature and residence time is Case 2 in Fig. 6. As we move up in temperature to point $C_2$, we notice that the low-temperature boundary has moved to a higher-temperature compared with $C_1$ at $Z_{\text{st}} =$ 0.064. The increased temperature necessary for the onset of soot can be explained by the lower fuel concentration at the $Z$ location of $C_2$, as indicated in Fig. 7b. Moving vertically from $C_2$ in Fig. 6, we note that the high-temperature boundary at $B_2$ is found at a lower temperature than that of the fuel/air case. This suggests that increasing $Z_{\text{st}}$ results in oxidizing species moving farther into the fuel-rich side of the peak temperature location, where they are available to oxidize potential soot precursor species. Note that the peak temperatures of these two flames are the same; however, as seen in Figs. 7a and, 7b, the location of peak temperature has shifted in mixture fraction space, as expected.

At $Z_{\text{st}} = 0.6$, we see from Fig. 6 that the low-temperature boundary represented by $C_3$ and the high-temperature boundary represented by $B_3$ have converged, indicating a sooting limit. If we first consider the low-temperature boundary, which is governed by finite-rate chemistry, there is sufficient fuel, temperature, and residence time for soot formation at $C_3$. However, by considering the boundary governed by the critical C/O ratio, we see that the increase in $Z_{\text{st}}$ has moved oxygen-containing species farther into the fuel-rich zone, thereby preventing soot formation at this location. We also note as before that the magnitude of the peak temperature has not changed, but the location of the peak temperature has shifted further in mixture fraction space, as indicated by $A_3$ in Fig. 7c.

This approach to describing the dynamics of soot inception in nonpremixed flames can be used to understand the controlling mechanisms for the sooting limits at different values of $Z_{\text{st}}$. In Fig. 8, plots similar to Fig. 6 are shown for flames corresponding to the inverse diffusion flames in Fig. 3. In Fig. 8a, a limit flame at $Z_{\text{st}} = 0.2$ with a flame temperature of 1800 K is shown. For this flame temperature and residence time the model suggests that the sooting limit is controlled by flame temperature, residence time, and fuel dilution alone, with no supplemental effect from the critical C/O ratio boundary. This can be seen as the $T_{\text{kin}}$ and $T_{\text{C/O}}$ curves intersect slightly above the point where $T_{\text{kin}}$ has reached its peak value of $Z_{\text{st}}$. That is, the model indicates that for a flame with a residence time of 0.022 s and a flame temperature of 1800 K the sooting limit is achieved at $Z_{\text{st}} = 0.2$ because there are insufficient time, temperature, and fuel—not because of the availability of oxygen-containing species, as characterized by the $T_{\text{C/O}}$ curve. This case is characteristic of the common case of a fuel/air or diluted-fuel/air flame. In Fig. 8b the model predicts a sooting limit at $Z_{\text{st}} = 0.25$ for a flame temperature of 1840 K. At this temperature and residence time the $T_{\text{kin}}$ and $T_{\text{C/O}}$ curves intersect below the point where $T_{\text{kin}}$ has reached its peak value of $Z_{\text{st}}$, suggesting that the boundary associated with oxygen-containing

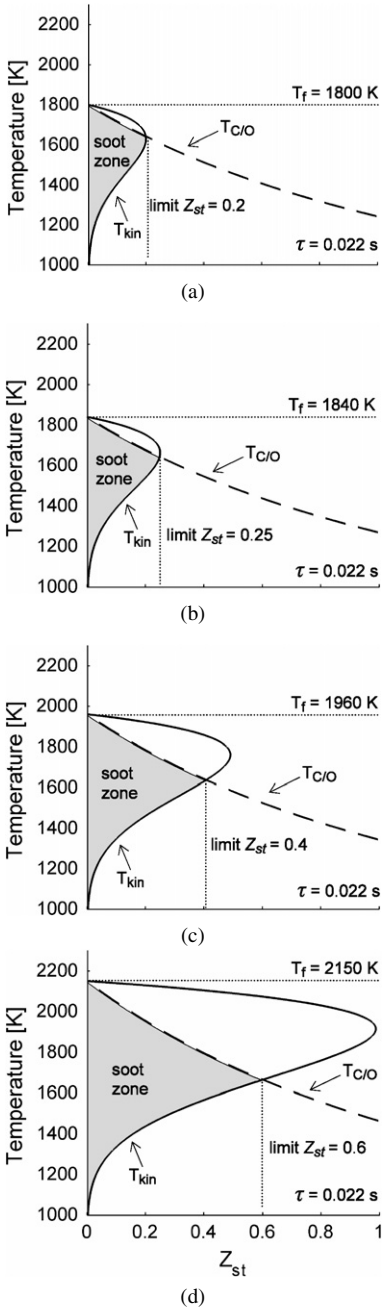


Fig. 8. Representation of the sooting zones of four flames with varying flame temperatures.

species (the critical C/O boundary) begins to affect sooting limits when $Z_{st} > 0.2$. In Fig. 8c the model predicts a sooting limit at $Z_{st} = 0.4$ for a flame temperature of 1960 K. Unlike the case in Fig. 8a, now the $T_{C/O}$ curve does not intersect the $T_{kin}$ curve until well below the point where $T_{kin}$ reaches its peak value of $Z_{st}$. In other words, the soot region is being substantially narrowed due to the critical C/O boundary. Fig. 8d demonstrates the dramatic effect of the critical C/O ratio boundary when the flame temperature is 2150 K at $Z_{st} = 0.65$. The $T_{kin}$ curve clearly extends beyond the realizable value of stoichiometric mixture fraction, suggesting that if the soot zone were considered to be strictly governed by pyrolysis then one would conclude that a sooting limit cannot exist for this flame temperature and residence time. On the contrary, a sooting limit is easily obtained for this flame because of the effect of the critical C/O ratio boundary. These results dramatically illustrate that flame structure governs soot inception in high-temperature oxygen-enriched/diluted-fuel (i.e., high-$Z_{st}$) flames.

## 4. Conclusion

A simple theory for predicting soot inception limits in nonpremixed flames has been presented that takes into account temperature, residence time, and gas composition. This model is an extension of previous soot inception models for diffusion flames in that it is applicable to high $Z_{st}$ combustion. This model is particularly useful for demonstrating how oxy–fuel combustion may lead to reduced soot formation without a compromise in flame temperature. By increasing the stoichiometric mixture fraction via the combination of oxygen enrichment and fuel dilution, soot formation is reduced and thus the sooting limit occurs at a higher temperature. This is found to occur in both normal and inverse flames. The sooting limit inception temperature is influenced by residence time, and when the effects of residence time are removed it is clear that increasing $Z_{st}$ affects both the normal and the inverse flames equally, indicating that flame configuration does not have a strong effect on the sooting limit. As demonstrated by the model, the effect of increasing $Z_{st}$ is to move the two boundaries of the soot formation zone towards each other. We find that the analysis made by Glassman [5], that the soot formation region is bounded by the isotherms corresponding to the incipient particle formation temperature and the stoichiometric flame temperature, is a good approximation for flames of very low $Z_{st}$, e.g., the typical fuel/air flame. The proposed sooting limit model reveals, however, that the high-temperature soot boundary can be moved well into the fuel side of the peak temperature for flames with higher $Z_{st}$. We find that oxygen enrichment begins to affect soot inception limits when $Z_{st} > 0.2$. Following the work of Sunderland et al. [11], the high-temperature soot boundary is described as the location where the local C/O ratio is equal to a critical value. The results of this work suggest that $(C/O)_{cr} = 0.53$ for the case

of ethylene, which is comparable to the global C/O ratio associated with premixed flames. It is demonstrated that the soot inception temperature is not a unique quantity, but rather is dependent upon residence time and $Z_{st}$. Finally, after comparing various measurements of soot inception temperature found in the literature, we find that there is an important distinction to be made between a soot inception temperature that is measured at the low-temperature boundary of a large soot formation zone ($T_{kin}$) and an inception temperature measured at the sooting limit, where the soot zone can be considered infinitely thin ($T_{lim}$).

## Acknowledgments

The authors are grateful to Drs. D.L. Urban, P.B. Sunderland, and B.-H. Chao and to D.P. Stocker for many helpful discussions. This work was funded by the National Aeronautics and Space Administration under Grant NCC3-1063 under the technical management of Dr. M.K. King.

## References

[1] A. Gomez, M.G. Littman, I. Glassman, Combust. Flame 70 (2) (1987) 225–241.
[2] K. Saito, A.S. Gordon, F.A. Williams, W.F. Stickle, Combust. Sci. Technol. 80 (1–3) (1991) 103–119.
[3] C.S. McEnally, L.D. Pfefferle, Combust. Flame 117 (1/2) (1999) 362–372.
[4] R.A. Dobbins, Combust. Flame 130 (3) (2002) 204–214.
[5] I. Glassman, Proc. Combust. Inst. 27 (1998) 1589–1596.
[6] I.M. Kennedy, Combust. Sci. Technol. 59 (1–3) (1988) 107–121.
[7] D.X. Du, R.L. Axelbaum, C.K. Law, Proc. Combust. Inst. 22 (1988) 387–394.
[8] K.C. Lin, G.M. Faeth, J. Propuls. Power 12 (4) (1996) 691.
[9] D.X. Du, R.L. Axelbaum, C.K. Law, Proc. Combust. Inst. 23 (1990) 1501–1507.
[10] J. Du, R.L. Axelbaum, Combust. Flame 100 (3) (1995) 367–375.
[11] P.B. Sunderland, D.L. Urban, D.P. Stocker, B.-H. Chao, R.L. Axelbaum, Combust. Sci. Technol. 176 (2004) 2143–2164.
[12] J.Y. Hwang, S.H. Chung, Combust. Flame 125 (1) (2001) 752.
[13] A. Kitajima, T. Hatanaka, M. Takeuchi, H. Torikai, T. Miyadera, Combust. Sci. Technol. 142 (2005) 72–88.
[14] B.M. Kumfer, S.A. Skeen, R. Chen, R.L. Axelbaum, Combust. Flame 147 (3) (2006) 233–242.
[15] G.W. Sidebotham, I. Glassman, Combust. Flame 90 (1992) 269–283.
[16] G.W. Sidebotham, I. Glassman, Combust. Sci. Technol. 81 (1992) 207–219.
[17] D.B. Makel, I.M. Kennedy, Combust. Sci. Technol. 97 (1994) 303–314.
[18] R.L. Vander Wal, Combust. Flame 26 (1996) 2269–2275.
[19] L.G. Blevins, R.A. Fletcher, B.A. Benner Jr., E.B. Steel, G.W. Mulholland, Proc. Combust. Inst. 29 (2002) 2325–2333.
[20] K.C. Oh, U.D. Lee, H.D. Shin, E.J. Lee, Combust. Flame 140 (2005) 249–254.
[21] C.R. Kaplan, K. Kailasanath, Combust. Flame 124 (1/2) (2001) 275–294.
[22] B.J. McBride, S. Gordon, Computer program for calculation of complex chemical equilibrium compositions and applications, NASA-RP-1311-P2, Cleveland, 1996.
[23] B.M. Kumfer, Design of diffusion flame structure for reduced soot using oxygen-enriched combustion, Dissertation, Washington University, St. Louis, MO, 2005.
[24] D.X. Du, R.L. Axelbaum, C.K. Law, Combust. Flame 102 (1/2) (1995) 11–20.
[25] I. Glassman, O. Nishida, G. Sidebotham, Critical Temperatures of Soot Formation, vol. 59, Springer-Verlag, Heidelberg, 1994, pp. 316–324.
[26] M.M. Harris, G.B. King, N.M. Laurendeau, Combust. Flame 64 (1) (1986) 99–112.
[27] J. Du, Effects of flame structure on soot-particle inception in diffusion flames, Dissertation, Washington University, St. Louis, MO, 1995.